https://doi.org/10.3311/PPme.23424

Periodica Polytechnica Mechanical Engineering, 68(4), pp. 291–303, 2024

The Effect of the Layup on the Stability of Composite Cylindrical Shells

Péter Máté[1*], András Szekrényes[1]

[1] Department of Applied Mechanics, Faculty of Mechanical Engineering, Budapest University of Technology and Economics, Műegyetem rkp. 3., H-1111 Budapest, Hungary
[*] Corresponding author, e-mail: peter.mate@mm.bme.hu

Received: 11 September 2023, Accepted: 04 November 2024, Published online: 14 November 2024

Abstract

Fiber reinforced plastic laminated composites have conquered greater and greater territory in the field of engineering in the past decades for their high strength to weight ratio. By varying the layup structure their behavior can easily be modified. One of the applications, that is investigated in this article is the slit tube or cylindrical shell, that used as a structural element undergoes bending. These shells indifferent from their material may experience the snap-through phenomenon (this depends both on the material and geometry) in which the shell flattens and loses its stability to bending. Depending on the layup bistable behavior also can be achieved, i.e., the shell would have two different shapes that are in equilibrium without any constraint. In this article the effect of the layup is investigated both on the bistable behavior and the snap-through phenomenon. Geometric limitations for the bistability are calculated based on a simple beam model from the literature. The same model is used to find the snap-through moment for these shells as a function of the orientation angle. It is also proven that the flattening of the shell cannot be evaded by changing the layup structure. The results are confirmed by FE simulations where applicable.

Keywords

composite cylindrical shell, stability, snap-through, bistability, FEM

1 Introduction

The polymer composite cylindrical shells presented in this article undergo pure bending, and their behavior is investigated under this load. The article mainly focuses on the simple beam model provided by Galletly and Guest [1], which although not accurate from a quantitative point of view, but provides a good qualitative description, and it is easy to handle numerically. Galletly and Guest [2] have also provided a more accurate shell model.

Cylindrical shells, tape-springs or storable tubular extendable members (STEMs, Rimrott [3]) have been researched in the past, one of the first good description for flat shells comes from Wuest [4], published in 1954, who provided a shell model for isotropic materials. They are used primarily as measuring tapes, made of steel. When made of isotropic materials, they are only monostable, although because of the snap-through phenomenon they can be easily coiled. Another feature of these shells is the propagation moment, that is a theoretically constant bending moment in a large longitudinal curvature interval of the buckled shell. This has been investigated by Martin et al. [5] based on the Ericksen bar [6].

In case of bistable behavior, the shell has two distinct, curved configurations, that are an extended state with a transverse curvature and a coiled state where the transverse curvature disappears (the shell flattens), and another longitudinal curvature appears. The bistable behavior can be achieved for the tape-springs made of isotropic material by plastic forming that leaves residual stresses in the shell. This was first described by Kebadze et al. [7] in 2004. The first analytical description for the composite bistable shells was given by Iqbal et al. [8], who determined the coiling and transverse curvatures by finding the energy minima of an infinitesimally small composite shell element. In the work of Galletly and Guest [1] it is shown that for an antisymmetric layup the second stable state coils in a helical manner. For further articles describing the bistable composite shell, the reader is referenced to [9–12]. Applications for tape springs include

Cite this article as: Máté, P., Szekrényes, A. "The Effect of the Layup on the Stability of Composite Cylindrical Shells", Periodica Polytechnica Mechanical Engineering, 68(4), pp. 291–303, 2024. https://doi.org/10.3311/PPme.23424

self-deployable structures, energy harvesting and morphing structures [11]. Another use of the slit tubes was presented by Seriani and Gallina [13], who have presented a STEM parallel robot.

Lately several articles aimed to describe the behavior of multistable, quasi-cylindrical composite shells with the help of the Föppl-von Kármán shell model, which can be used to create models with a reduced number of degrees of freedom for better handling [14, 15]. Brunetti et al. [16] also confirmed that the reduced order model is able to predict the elastic energy content and the stable shapes of the clamped shells with acceptable accuracy. Brunetti et al. [17] also examined the nonlinear dynamics of these clamped cantilever shells, to enhance the energy harvesting capabilities, which were experimentally investigated by Mitura et al. [18].

In the article based on the model of Galletly and Guest [1] several calculations have been caried out to analyze the effect of the layup. A method will be presented on how to use this model to determine the equilibrium trajectories of the shell under pure longitudinal bending. It will be shown how the snap-through moment depends on the layup and cross-section geometry. In the last section a criterion for the bistable behavior is also introduced.

2 Modelling methods

In this section the model for the composite slit tube provided by Galletly and Guest [1] will be presented for the reader to get familiar with the expressions and methods used later in the article. In Section 2.3 a finite element (FE) model is presented, the results of which are compared to the results obtained with the beam model.

2.1 Beam model

The model treats the shell as a thin-walled section. The parameters and geometry of the shell are given in Fig. 1.

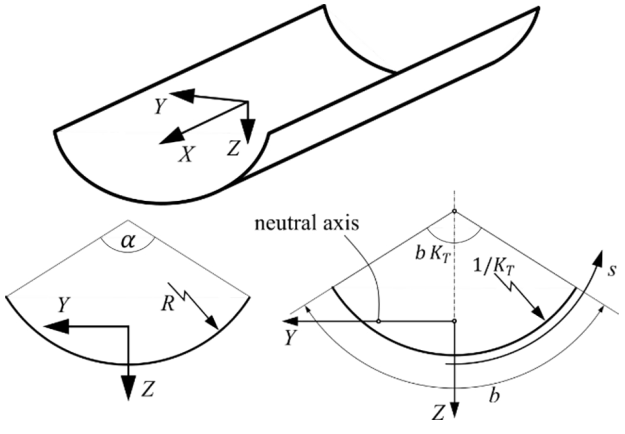

Fig. 1 The geometry and parametrization of the cylindrical shell

The four main loads of the cylindrical shell are presented in Fig. 2. These are tension (N), torsional moment (T), longitudinal bending moment (M_L), and transverse bending moment (M_T). In Fig. 3 the four deformation modes are also presented.

The assumptions include that there is no change in the deformation parameters along the beam, which means it deforms uniformly, and that the cross-section never loses the circular shape. Of all the deformation modes shear and bending around the Z axis are neglected. This leaves four deformations that need to be considered: E_x; ϕ; K_L; K_T, which are the longitudinal strain of the beam, the twist around X axis per unit length, longitudinal curvature, and cross-section curvature. It is important to emphasize that restricting the shape of the cross-section to a circular arc makes the model stiffer to bending than the reality [19, 20].

The local strains and curvatures used in the model, derived in [1] are given in Eqs. (1)–(4).

$$\varepsilon_x(s) = E_x - \frac{K_L}{K_T}\left(\frac{2}{bK_T}\sin\left(\frac{bK_T}{2}\right) - \cos(sK_T)\right) + 2\frac{\phi^2}{K_T^2}\sin^2\left(\frac{sK_T}{2}\right) \tag{1}$$

$$\kappa_x(s) = K_L\cos(sK_T) \tag{2}$$

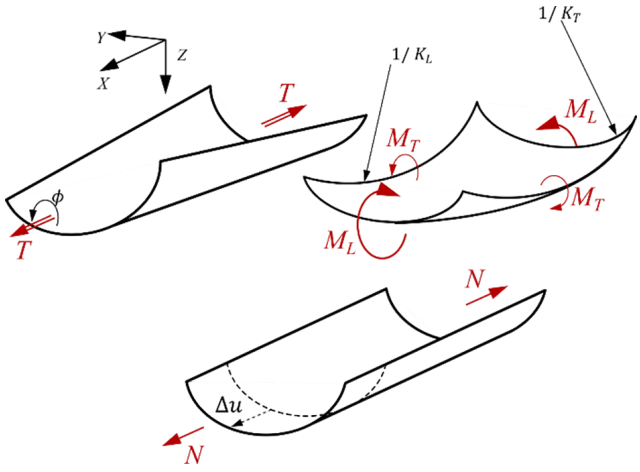

Fig. 2 The loads and deformation modes of the shell considered in the model

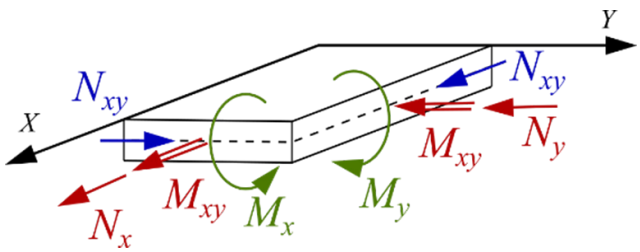

Fig. 3 The forces acting on an infinitesimally small section of the shell: Of these stress resultants N_y and N_{xy} are to be set to zero.

$$\kappa_y(s) = K_T - \frac{1}{R} \tag{3}$$

$$\kappa_{xy}(s) = -2\phi \tag{4}$$

Equations (1)–(4) are approximated by Galletly and Guest [1] by substituting the trigonometrical functions with their truncated series. The simplified expressions given in [1] are presented in Eqs. (5), (6). Note that the formulas for κ_y and κ_{xy} remain unchanged.

$$\varepsilon_x(s) \approx E_x + \frac{K_L K_T}{2}\left(\frac{b^2}{12} - s^2\right) + \frac{\phi^2 s^2}{2} \tag{5}$$

$$\kappa_x \approx K_L \tag{6}$$

The constitutive equation for the laminated plate in the linear region is given in Eq. (7), by using the ABD-matrix [1, 21]. Here $\boldsymbol{A}$, $\boldsymbol{B}$, and $\boldsymbol{D}$ are the extensional, extensional-bending coupling stiffness, and bending stiffness matrices [21]. The forces and bending moments (stress resultants) considered in this equation are presented in Fig. 3.

$$\begin{bmatrix} N_x \\ N_y \\ N_{xy} \\ M_x \\ M_y \\ M_{xy} \end{bmatrix} = \begin{bmatrix} \boldsymbol{A} & \boldsymbol{B} \\ \boldsymbol{B} & \boldsymbol{D} \end{bmatrix} \begin{bmatrix} \varepsilon_x \\ \varepsilon_y \\ \gamma_{xy} \\ \kappa_x \\ \kappa_y \\ \kappa_{xy} \end{bmatrix} \tag{7}$$

Since in this model there is no cross directional load and shearing force present, we can set these terms to be zero; thus, $N_{xy} = 0$ and $N_y = 0$. By setting these zero, the constitutive equation can be rearranged in the form of Eq. (8).

$$\begin{bmatrix} N_x \\ M_x \\ M_y \\ M_{xy} \\ 0 \\ 0 \end{bmatrix} = \begin{bmatrix} A_{11} & B_{11} & B_{12} & B_{16} & A_{12} & A_{16} \\ B_{11} & D_{11} & D_{12} & D_{16} & B_{12} & B_{16} \\ B_{12} & D_{12} & D_{22} & D_{26} & B_{22} & B_{26} \\ B_{16} & D_{16} & D_{26} & D_{66} & B_{26} & B_{66} \\ A_{12} & B_{12} & B_{22} & B_{26} & A_{22} & A_{26} \\ A_{16} & B_{16} & B_{26} & B_{66} & A_{26} & A_{66} \end{bmatrix} \begin{bmatrix} \varepsilon_x \\ \kappa_x \\ \kappa_y \\ \kappa_{xy} \\ \varepsilon_y \\ \gamma_{xy} \end{bmatrix} \tag{8}$$

From here the membrane strains ε_y and γ_{xy} can be expressed as a function of the other four remaining strains and curvatures. For this the ***ABD*** matrix can be divided into three submatrices, namely: $\boldsymbol{K}_0$, $\boldsymbol{K}_1$ and $\boldsymbol{K}_2$. These are given in Eqs. (9)–(11). The reordered system of equation is given in Eq. (12).

$$\boldsymbol{K}_0 = \begin{bmatrix} A_{11} & B_{11} & B_{12} & B_{16} \\ B_{11} & D_{11} & D_{12} & D_{16} \\ B_{12} & D_{12} & D_{22} & D_{26} \\ B_{16} & D_{16} & D_{26} & D_{66} \end{bmatrix} \tag{9}$$

$$\boldsymbol{K}_1 = \begin{bmatrix} A_{12} & B_{12} & B_{22} & B_{26} \\ A_{16} & B_{16} & B_{26} & B_{66} \end{bmatrix} \tag{10}$$

$$\boldsymbol{K}_2 = \begin{bmatrix} A_{22} & A_{26} \\ A_{26} & A_{66} \end{bmatrix} \tag{11}$$

$$\begin{bmatrix} N_x \\ M_x \\ M_y \\ M_{xy} \\ 0 \\ 0 \end{bmatrix} = \begin{bmatrix} \boldsymbol{K}_0 & \boldsymbol{K}_1^{\mathrm{T}} \\ \boldsymbol{K}_1 & \boldsymbol{K}_2 \end{bmatrix} \begin{bmatrix} \varepsilon_x \\ \kappa_x \\ \kappa_y \\ \kappa_{xy} \\ \varepsilon_y \\ \gamma_{xy} \end{bmatrix} \tag{12}$$

Using these, the stress resultants relevant in this model can be expressed as a function of the relevant strains and curvatures, given in Eq. (13). The new, reduced stiffness matrix $\boldsymbol{K}^*$ [1] is given in Eq. (14) and Eq. (15).

$$\begin{bmatrix} N_x \\ M_x \\ M_y \\ M_{xy} \end{bmatrix} = \boldsymbol{K}^* \begin{bmatrix} \varepsilon_x \\ \kappa_x \\ \kappa_y \\ \kappa_{xy} \end{bmatrix} \tag{13}$$

$$\boldsymbol{K}^* = \boldsymbol{K}_0 - \boldsymbol{K}_1^{\mathrm{T}} \cdot \boldsymbol{K}_2^{-1} \cdot \boldsymbol{K}_1 \tag{14}$$

$$\boldsymbol{K}^* = \begin{bmatrix} A_{11}^* & B_{11}^* & B_{12}^* & B_{16}^* \\ B_{11}^* & D_{11}^* & D_{12}^* & D_{16}^* \\ B_{12}^* & D_{12}^* & D_{22}^* & D_{26}^* \\ B_{16}^* & D_{16}^* & D_{26}^* & D_{66}^* \end{bmatrix} \tag{15}$$

By substituting Eqs. (1)–(4) or Eqs. (3)–(6) into Eq. (15) one can express the stress resultants as a function of the beam deformation parameters. From here, properly integrating these over the cross-section yields the loads on the body. Let $\boldsymbol{N}^{\mathrm{T}} := [N_x\ M_x\ M_y\ M_{xy}]$ and $\boldsymbol{\varepsilon}^{\mathrm{T}} := [\varepsilon_x\ \kappa_x\ \kappa_y\ \kappa_{xy}]$. The tension on the beam is assumed to be zero throughout the analysis. This allows the expression of as a function of the other deformation parameters and thus it can be eliminated. The definition of the global tension (as named in the original work [1]) is presented in Eq. (16).

$$P = \int_{-\frac{b}{2}}^{\frac{b}{2}} N_x \, ds \tag{16}$$

Now, the beam loads can be determined with the help of virtual work, which yields the formulas given in Eqs. (17)–(19).

$$T = \int_{-\frac{b}{2}}^{\frac{b}{2}} \frac{\partial \boldsymbol{\varepsilon}^{\mathrm{T}}}{\partial \phi} \cdot \boldsymbol{N}\, ds \tag{17}$$

$$M_T = \int_{-\frac{b}{2}}^{\frac{b}{2}} \frac{\partial \boldsymbol{\varepsilon}^{\mathrm{T}}}{\partial K_T} \cdot \boldsymbol{N}\, ds \tag{18}$$

$$M_L = \int_{-\frac{b}{2}}^{\frac{b}{2}} \frac{\partial \boldsymbol{\varepsilon}^{\mathrm{T}}}{\partial K_L} \cdot \boldsymbol{N}\, ds \tag{19}$$

To calculate the nonzero moments on the beam (T, M_L, M_T), one must substitute Eqs. (3)–(6) into Eqs. (17)–(19) and express the vector of the stress resultants $\boldsymbol{N}$ as a function of strains and curvatures using Eq. (13). After integration, the torsional, longitudinal and transverse moment can be given in the form of Eqs. (20)–(22):

$$\begin{aligned} T = {} & A_{11}^{*}\left(\phi^2 - K_L K_T\right)\phi\frac{b^5}{360} - 2D_{16}^{*}bK_L \\ & -2D_{16}^{*}b\left(K_T - \frac{1}{R}\right) + 4\left(D_{66}^{*} - \frac{B_{16}^{*}}{A_{11}^{*}}\right)b\phi, \end{aligned} \tag{20}$$

$$\begin{aligned} M_L = {} & -A_{11}^{*}\left(\phi^2 - K_L K_T\right)K_T\frac{b^5}{720} + D_{11}^{*}bK_L \\ & +D_{12}^{*}b\left(K_T - \frac{1}{R}\right) - 2D_{16}^{*}b\phi, \end{aligned} \tag{21}$$

$$\begin{aligned} M_T = {} & -A_{11}^{*}\left(\phi^2 - K_L K_T\right)K_L\frac{b^5}{720} + D_{12}^{*}bK_L \\ & +D_{22}^{*}b\left(K_T - \frac{1}{R}\right) - 2D_{26}^{*}b\phi. \end{aligned} \tag{22}$$

For further details on the derivation of this model, the reader is referred to the paper of Galletly and Guest [1].

2.2 Material properties

The material used here is a fiber reinforced plastic which has been used for the numerical calculations performed both by Iqbal et al. [8] and Galletly and Guest [1]. They use a 5-layer symmetric and an antisymmetric layup with a ±45° orientation angle, with a 0° layer in the middle. These are defined as [+45°, −45°, 0°, +45°, −45°] for the antisymmetric and [+45°, −45°, 0°, −45°, +45°] for the symmetric. The reduced stiffness matrices for the laminates are given in Eqs. (23), (24), for the antisymmetric and symmetric cases, respectively, as given in the original work [1].

$$\boldsymbol{K}_{as}^{*} = \begin{bmatrix} 8757 & 0 & 0 & 136.1 \\ 0 & 819 & 616 & 0 \\ 0 & 616 & 799 & 0 \\ 136.1 & 0 & 0 & 643 \end{bmatrix} \tag{23}$$

$$\boldsymbol{K}_{s}^{*} = \begin{bmatrix} 8757 & 0 & 0 & 0 \\ 0 & 868 & 665 & 345 \\ 0 & 665 & 848 & 345 \\ 0 & 345 & 345 & 681 \end{bmatrix} \tag{24}$$

The A_{ij}^{*} elements have a unit of [N/mm], the B_{ij}^{*} is given in [N] and the D_{ij}^{*} components have [N mm] as a unit of measurement. One can see that both stiffness matrices give chance to significant simplifications. For the symmetric layup every $B_{ij}^{*} = 0$. For The antisymmetric layup $B_{11}^{*} = B_{12}^{*} = D_{16}^{*} = D_{26}^{*} = 0$.

For one to be able to investigate the effect of the orientation angle, the basic stiffness matrix of such an orthotropic layer and the wall thickness of the shell must be known. The thickness for these reduced stiffness matrices was 1.05 mm. As the basic elasticity parameters were not given in [1], this was obtained by calculating the $\boldsymbol{K}_{as}^{*}$ matrix parametrically, and then equating it to the data given in Eq. (23). As some elements of the reduced stiffness matrix are nonlinear in the nonzero elements of $\boldsymbol{C}$ matrix, a numerical solver was used to obtain $\{C_{11}, C_{22}, C_{12}, C_{33}\}$. Thus, the stiffness matrix for a layer is given in Eq. (25).

$$\boldsymbol{C} = \begin{bmatrix} 28028.7 & 767.7 & 0 \\ 767.7 & 2133.3 & 0 \\ 0 & 0 & 949.9 \end{bmatrix} [\mathrm{MPa}] \tag{25}$$

The elasticity parameters for the FE simulations were calculated from the stiffness matrix of the orthotropic layer [21]. These are given in Table 1, both for the material used in [1] (Material 1) and the material used in [15, 16] (Material 2).

2.3 Finite Element model

In this section a finite element model is presented, that was used to calculate bending characteristics, snap-through moment and bistability limits for composite shells with different layups. The purpose of the FE model is to

Table 1 Material elasticity parameters

Material	E_{11} [MPa]	E_{22} [MPa]	G_{12} [MPa]	ν_{12} [–]
Material 1	27752.4	2112.27	949.9	0.359
Material 2	130710	6360	4180	0.32

validate the behavior predicted by the calculations based on the model of Galletly and Guest [1]. The simulations were carried out in ABAQUS CAE environment.

The model simulates a pure bending scenario, in which a symmetry constraint is applied to one end of the modeled beam section, while a rotation constraint is applied to the other end. Both constrained cross-sections are free to deform in their plane, as shown in Fig. 4. The rotational displacement load was applied through a reference point which is kinematically coupled to the nodes of the cross-section, as presented in Fig. 4. A similar model was used to investigate the behavior of isotropic cylindrical shells and to validate various pure bending models in [22]. Unfortunately, the simulations were not convergent for the symmetric layup without constraining the twisting motion of the cross-section, thus results are available only for the antisymmetric layup.

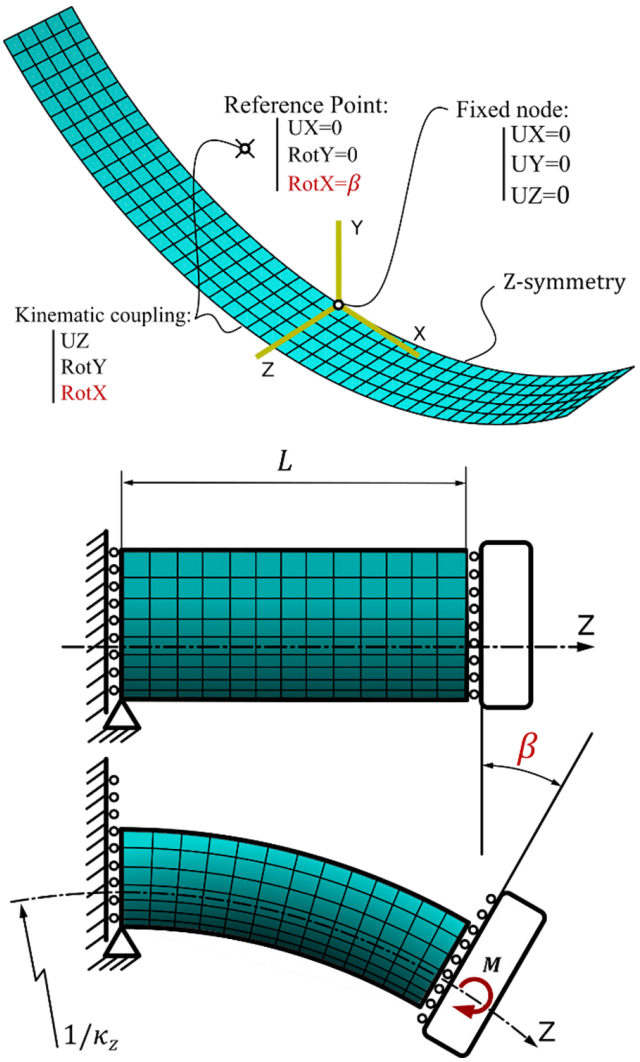

Fig. 4 The ABAQUS finite element model of the pure bending of the composite cylindrical shell

3 Bending characteristics

One of the main interests discussed in this article is the bending characteristics of such a cylindrical shell. Here we assume that the only load on the shell is the longitudinal bending moment. This assumption is contested later when the symmetric and antisymmetric layups are being discussed. In the former case an additional torsional moment must be considered too. We assume uniform bending throughout the investigation.

3.1 Dimensionless variables

Similarly to [1], the following dimensionless variables will be introduced: k_l, k_t, φ. These are the dimensionless longitudinal moment, dimensionless transverse moment, and the dimensionless twist, whose definition is given in Eq. (26).

$$\begin{cases} k_l = K_L R \\ k_t = K_T R \\ \varphi = \phi R \end{cases} \tag{26}$$

This does not give dimensionless moments, since it leaves the cross-section parameters (R and α or R and b) in the equation. Trials to create dimensionless moments failed to the complicated buildup of the stiffness matrix, which includes terms with different units, and different powers of wall thickness. The form of Eqs. (20)–(22) with dimensionless variables is presented in Eqs. (27)–(29). To obtain this form, one must substitute Eq. (26) into Eqs. (20)–(22), and the cross-section arc-length b must also be substituted by $R\alpha$. Here, α and R are the unloaded cross-section's central angle and radius, as indicated in Fig. 1.

$$\begin{aligned} T = {} & A_{11}^{*}\left(\varphi^2 - k_l k_t\right)\varphi \frac{\alpha^5 R^5}{360} \\ & -2\alpha\left(D_{16}^{*}k_y - 2D_{66}^{*}\varphi + D_{26}^{*}\left(k_t - 1\right)\right) - 4\frac{B_{16}^{*\,2}}{A_{11}^{*}}\alpha\varphi \end{aligned} \tag{27}$$

$$\begin{aligned} M_L = {} & A_{11}^{*}k_t^2 k_l \frac{\alpha^5 R^2}{720} + D_{11}^{*}\alpha k_l + D_{12}^{*}\alpha\left(k_t - 1\right) - 2D_{16}^{*}\alpha\varphi \\ & -A_{11}^{*}k_t\varphi^2 \frac{\alpha^5 R^2}{720} \end{aligned} \tag{28}$$

$$\begin{aligned} M_T = {} & A_{11}^{*}k_t k_l^2 \frac{\alpha^5 R^2}{720} + D_{12}^{*}\alpha k_l + D_{22}^{*}\alpha\left(k_t - 1\right) - 2D_{26}^{*}\alpha\varphi \\ & -A_{11}^{*}k_l\varphi^2 \frac{\alpha^5 R^2}{720} \end{aligned} \tag{29}$$

3.2 Equilibrium equations

To find the equilibrium of the beam under uniform bending one needs to consider $M_T = 0$ which should always be true. Since we want to find the response of the beam given to a longitudinal bending moment, the longitudinal beam curvature (k_l) will be expressed both from Eq. (28) and Eq. (29) with keeping the transverse moment zero. Equation (28) yields a single result that is given in Eq. (30) and named $k_l^{(0)}$. Equation (29) yields two solutions, which are $k_l^{(1)}$ and $k_l^{(2)}$ given in Eqs. (31), (32).

$$k_l^{(0)} = \frac{M_L + D_{12}^*\alpha\left(1-k_t\right) + 2D_{16}^*\alpha\varphi + \frac{1}{720}A_{11}^*R^2\alpha^5\varphi^2}{\alpha\left(D_{11}^* + \frac{1}{720}A_{11}^*k_t^2R^2\alpha^4\right)} \tag{30}$$

$$k_l^{(1)} = \frac{-720D_{12}^* + A_{11}R^2\alpha^4\varphi^2}{2A_{11}^*k_tR^2\alpha^4} - \frac{\sqrt{2880A_{11}^*k_tR^2\alpha^4\left(D_{22}^*\left(1-k_t\right)+2D_{26}^*\varphi\right)+\left(720D_{12}^*-A_{11}^*R^2\alpha^4\varphi^2\right)^2}}{2A_{11}^*k_tR^2\alpha^4} \tag{31}$$

$$k_l^{(2)} = \frac{-720D_{12}^* + A_{11}R^2\alpha^4\varphi^2}{2A_{11}^*k_tR^2\alpha^4} + \frac{\sqrt{2880A_{11}^*k_tR^2\alpha^4\left(D_{22}^*\left(1-k_t\right)+2D_{26}^*\varphi\right)+\left(720D_{12}^*-A_{11}^*R^2\alpha^4\varphi^2\right)^2}}{2A_{11}^*k_tR^2\alpha^4} \tag{32}$$

Finding the transverse curvature values where $k_y^{(0)}$ equals either $k_l^{(1)}$ or $k_l^{(2)}$ will yield the equilibrium state(s) of the cylindrical shell for a given bending moment M_L. However, these equations still contain the twist of the beam, for which one either sets the torsional moment or the twist to be zero, depending on the defined boundary conditions of the beam. Expressing k_l yields a fourth solution for the longitudinal curvature, that is given in Eq. (33).

$$k_l^{(3)} = \frac{-\frac{T}{2\alpha} + D_{26}^*\left(1-k_t\right) - \frac{2B_{16}^{*\,2}}{A_{11}^*}\varphi + 2D_{66}^*\varphi + \frac{1}{720}A_{11}^*R^2\alpha^4\varphi^3}{\left(D_{16}^* + \frac{1}{720}A_{11}^*k_t\varphi R^2\alpha^4\right)} \tag{33}$$

3.3 The antisymmetric layup

The antisymmetric layup is the easier to treat, since if one assumes a zero torsional moment ($T = 0$), three solutions emerge for the dimensionless twist, from which according to [1] $\varphi = 0$ is the stable one. Using this, one can use only Eqs. (30)–(32) to find the equilibrium. Plotting the $k_l^{(1)}$ and $k_l^{(2)}$ characteristics along with the bending moment dependent $k_l^{(0)}$ characteristic shows the behavior of the system. This is given in Fig. 5. In Fig. 5 one can already see for the $\alpha = 120°$ case that the shell has bistable property, for the bending moment dependent characteristic with crosses $k_l^{(1)}$ three times. From these solutions one is the initial state with $k_t = 1$ and $k_l = 0$, the other two are additional states, from which the middle one is an unstable one. As one increases the bending moment in either direction, at a certain point three solutions appear, then the two solutions with higher k_t values join and only one remains, with almost zero transverse curvature and a high longitudinal one. The unification of the solutions corresponds to the snap-through, when the shell loses stability and flattens.

For the model [1] is based on the polynomial approximation of the trigonometric functions, we have derived the equilibrium equations from Eqs. (17)–(19) without the approximation and compared the results for the three characteristics given in Eqs. (30)–(32). It yielded only a few percent relative error in the k_t region close to unity. Error closer to the flattened state was negligible, which makes it perfectly suitable for these calculations. Note that the model error is greater than the error of the approximation. This is presented in Fig. 6.

One can plot the results of the uniform longitudinal bending in the $k_l - M_L$ plane. For this we use parametric plot, where the curve parameter is the transverse curvature, with $k_t \in (0,1]$. The abscissa would be calculated using Eqs. (31), (32), while the ordinate is given by inserting either Eq. (31) or Eq. (32) into Eq. (28). Results for some geometries are given in Fig. 7.

Here one can observe the effect of the cross-section size on the snap-through moment. It is also observable that the curvature-bending moment characteristic for some cases

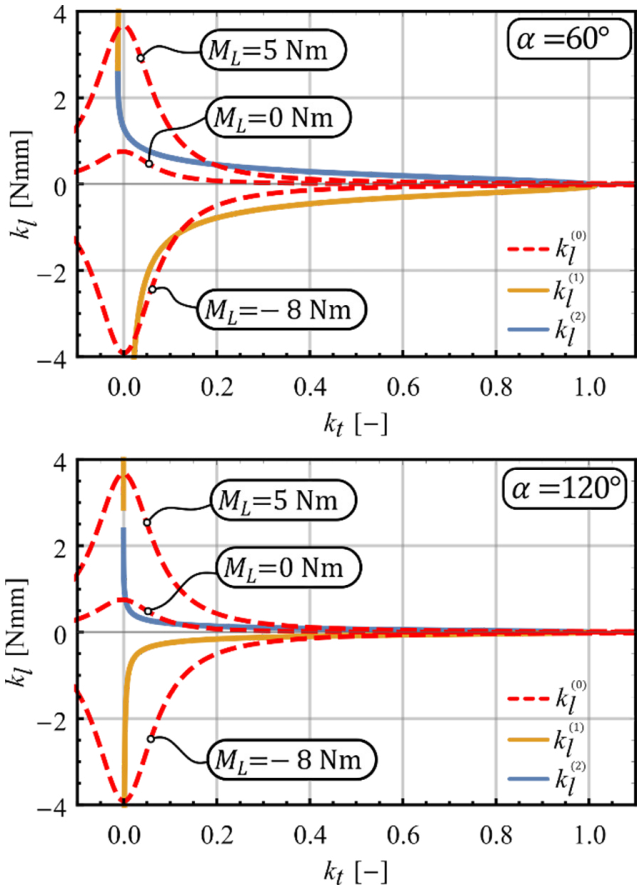

Fig. 5 The characteristic curves for the antisymmetric layup, for two initial central angles and R = 25 mm: Equilibrium is where the dashed curve crosses the moment independent characteristics.

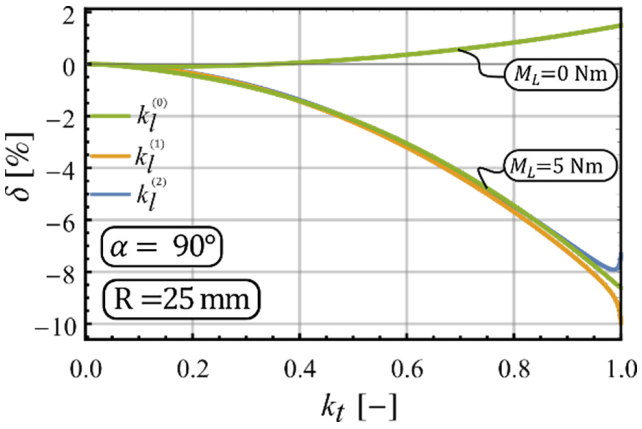

Fig. 6 The error of the approximation for a given setup: The trend was similar for any angle. The $k_l^{(0)}$ error rapidly converges to the error of the other two with the bending moment.

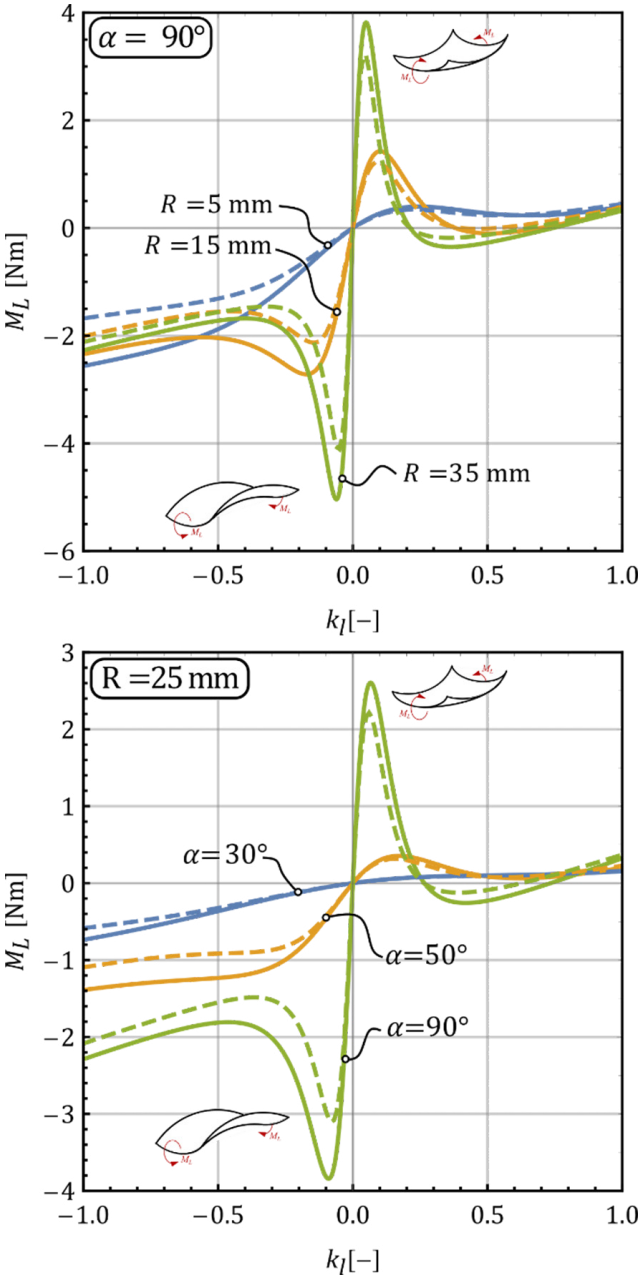

Fig. 7 The curvature- bending moment characteristics for several geometric configurations for the antisymmetric layup: The dashed lines represent the FE simulation results.

becomes monotonic. This also causes the shell to flatten, although without stability loss. We have conducted calculations on the snap-through moments for different orientation angles for the antisymmetric layup. These revealed that there is an oscillation in the peak bending moment the beam can withstand before stability loss. In a real-world scenario the positive sense bending (that causes a positive beam curvature in the model) is highly unstable in nature, thus only the reverse bending (negative bending moment and beam curvature) was investigated. The results for the stacking sequence in [1] with *Material 1* are presented in Fig. 8, while the results for the stacking sequence given in [16] with *Material 2* are shown in Fig. 9.

Fig. 8 and Fig. 9 reveal another interesting behavior which can also be seen in the FE simulation results: for layups without a fixed-orientation middle layer,

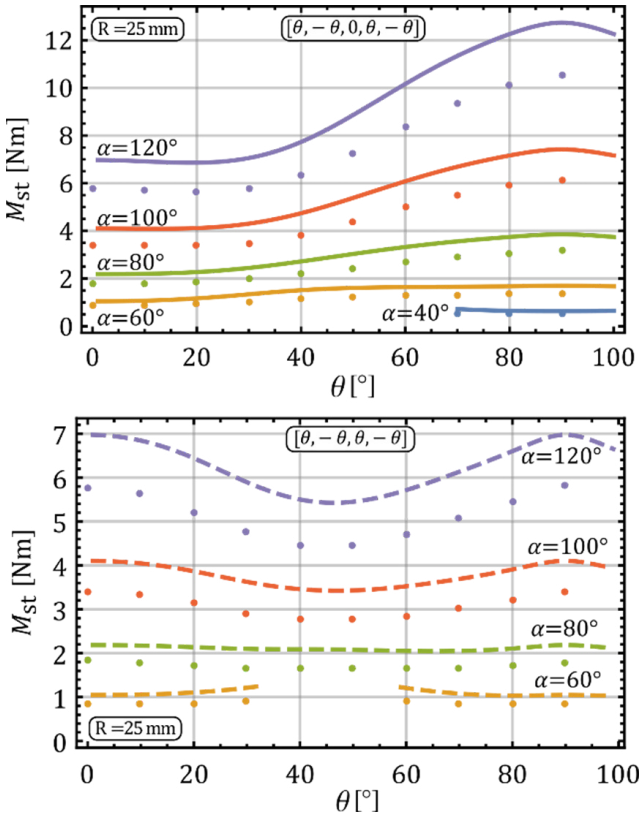

Fig. 8 The effect of the layup orientation angle on the snap-through moment for different cross-section angles and layups (Material 1), compared to FE simulations

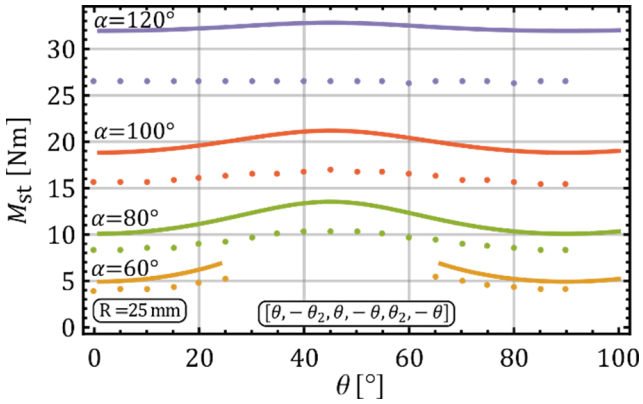

Fig. 9 The effect of the layup orientation angle on the snap-through moment for different cross-section angles (Material 2), compared to FE results

a cross-section angle exists, for which the layup orientation has practically no effect on the snap-through moment. However, the critical beam curvature where the peak bending moment appears may change significantly. Fig. 10 shows how the bending moment-curvature function changes with the layup angle θ, for Material 2 and the layup of [16]. The bending characteristics are calculated for a cross-section geometry, for which the layup angle practically does not change the snap-through moment.

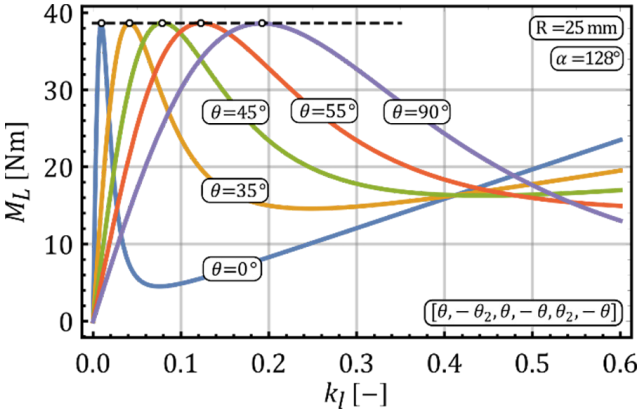

Fig. 10 The effect of the layup orientation angle on the bending characteristic for opposite sense bending

This configuration for example allows the changing the stiffness of the beam, while keeping the geometry and load bearing capacity constant.

To increase the load bearing capacity of such a shell, and to avoid the snap-through phenomenon, one could try to shift the singularity to the right in the $k_l^{(1,2)}$ characteristics. However, this is not possible even based on the not simplified model. The equation for the roots of the denominator in the model without approximation is given in Eq. (34). With increasing α one can produce a root above zero, however this is not in the region of practical interest.

$$A_{11}^{*}R\left(B_{11}^{*}k_t + A_{11}^{*}R\right)\begin{pmatrix}\left(16-2kt^2\alpha^2\right)\left(1-\cos k_t\alpha\right)\\ -kt^2\alpha^2 - 7k_t\alpha\sin k_t\alpha\end{pmatrix} = 0 \qquad (34)$$

3.4 The symmetric layup

With the symmetric layup the equations are somewhat more complicated. Setting the torsional moment to zero does not allow us to neglect the torsional deformation mode of the beam. In this case, all four equations (Eqs. (30)–(33)) need to be considered, as given in Eq. (35):

$$\begin{cases} k_l^{(0)}\left(M_L, k_t, \varphi\right) = k_l^{(1)}\left(k_t, \varphi\right) = k_l^{(3)}\left(T=0, k_t, \varphi\right) \\ k_l^{(0)}\left(M_L, k_t, \varphi\right) = k_l^{(2)}\left(k_t, \varphi\right) = k_l^{(3)}\left(T=0, k_t, \varphi\right) \end{cases}. \qquad (35)$$

These equations in Eq. (35) were taken into two pieces: $k_l^{(0)} = k_l^{(1,2)}$ and $k_l^{(1,2)} = k_l^{(3)}$. The system of equations was solved numerically for a cross-section angle of 135°, radius of 25 mm, with the symmetrical layup from [1] and Material 1. The solution yields two separate curves which do not cross each other, when plotted in the space of dimensionless torsion, dimensionless cross-section curvature and bending moment, as given in Fig. 11. Decreasing this angle will shrink the second, isolated trajectory, and will make it ultimately disappear. Twist is inevitable

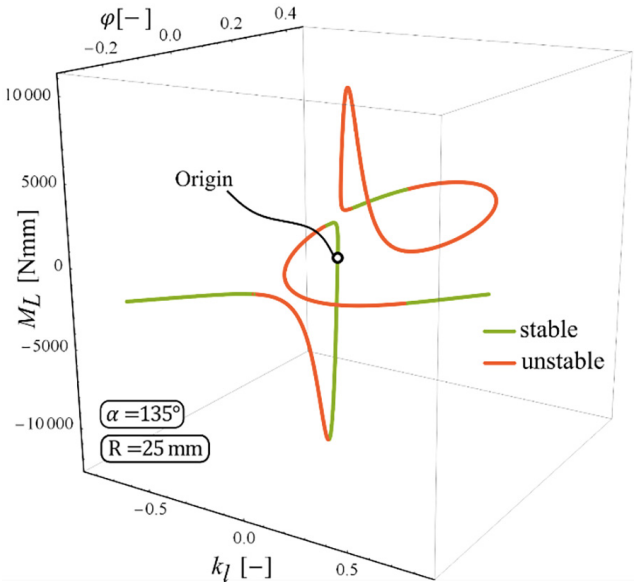

Fig. 11 The bending characteristic of the symmetric layup: One can observe two separate curves which do not cross each other.

without any additional constraints. For each point the stability is defined with the tangent stiffness matrix. If it is positive definite, the equilibrium is stable [1]. This matrix is defined as in Eq. (36).

$$\boldsymbol{H} = \begin{bmatrix} \frac{\partial}{\partial \varphi} & \frac{\partial}{\partial k_l} & \frac{\partial}{\partial k_t} \end{bmatrix}^{\mathrm{T}} \cdot \begin{bmatrix} T & M_L & M_T \end{bmatrix} \tag{36}$$

4 Bistability limits

As shown by Galletly and Guest [1] the bistable behavior does not only depend on the layup, but the macroscopic geometric properties too. For a given layup there are geometry combinations that can produce a second stable configuration. For the material properties given in [1, 8] we have found numerically the limit curve of the cross-section radius (R_{min}) as a function of the initial cross-section central angle (α), above which the shell will have a second stable state. The numerical analysis revealed that the curves themselves when plotted in a logarithmic plot have a highly linear trend, as shown in Fig. 12. This suggested that there may be an analytical solution to them, which was ultimately found, and it is given in Eq. (39) for the antisymmetric layup. Finding proper solutions for the symmetric layup was hard even numerically since the twisting of the beam cannot be eliminated. For the latter, in some bistable configurations, several equilibrium solutions are found simultaneously that are either unstable or need unrealistic deformations (additionally to the two realizable stable states).

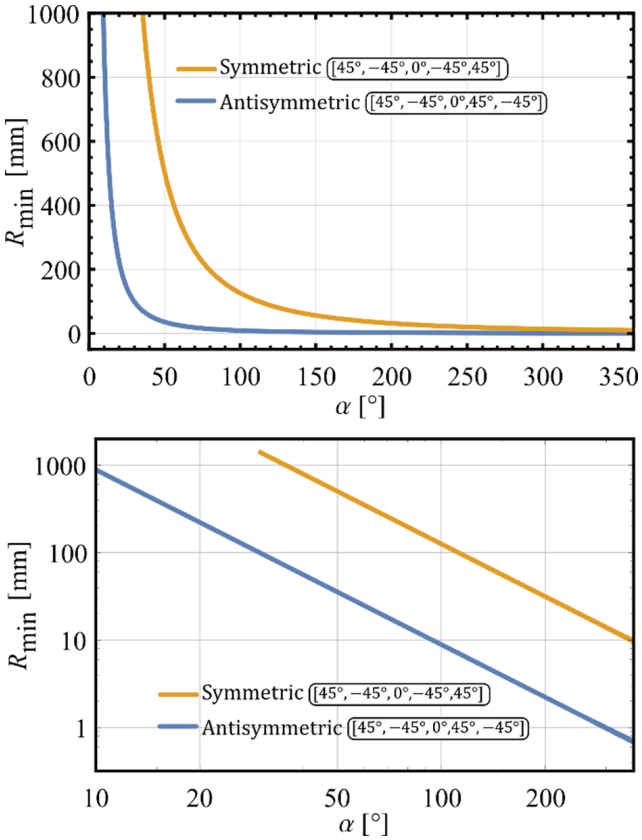

Fig. 12 The bistability limits calculated for the 45° symmetric and antisymmetric layup with Material 1. Bistable configurations can be found above the curves.

4.1 Bistability limit of the antisymmetric layup

For the antisymmetric layup, as seen before, stable solution exists only when there is no twist in the beam, i.e., $\varphi = 0$. It is easy to see that $k_l^{(0)}$ can only be positive for $M_L = 0$ in the region of interest i.e., $k_t \in [0,1)$. That would mean that $k_l^{(2)}$ and $k_l^{(0)}$ must be equal, which leads to Eq. (37):

$$k_l^{(2)}(k_t) - k_l^{(0)}(k_t) = 0\,. \tag{37}$$

The initial method was solving in Eq. (37) numerically for several R values for a given α and see where the second stable and unstable solutions appear or disappear. The limiting value for the initial radius has been found by bisection method.

For this special case we have found 5 k_t solutions for Eq. (37). From these, one is $k_t = 1$, the initial state, two others are complex roots and the other two may be complex or real depending on the $[R; \alpha]$ combination. These formulas are lengthy; thus, they will not be published in the article. A square root function inside the solutions must be investigated to find whether complexity is present or not. This governing equation is given in Eq. (38).

The solutions for Eq. (38) represent the boundary between the mono- and bistable geometries:

$$\begin{aligned}&-14745600D_{11}^{*4}D_{22}^{*2}+23040A_{11}^{*}D_{11}^{*2}D_{12}^{*2}D_{22}^{*}R^2\alpha^4\\&+3A_{11}^{*2}D_{12}^{*4}R^4\alpha^8-20480D_{11}^{*3}D_{22}^{*}\begin{pmatrix}-720D_{12}^{*2}\\+A_{11}D_{22}R^2\alpha^4\end{pmatrix}=0.\end{aligned}\tag{38}$$

The solution of the polynomial yields 4 solutions for the smallest radius R in which there is only one positive real solution. The resulting formula for $R_{\min}$ is given in Eq. (39):

$$\begin{aligned}&R_{\min}(\alpha)=\alpha^{-2}\frac{16}{\sqrt{A_{11}^{*}D_{12}^{*2}}}\sqrt{\frac{5}{3}}\\&\cdot\left(\begin{matrix}D_{11}^{*2}D_{22}^{*}\left(8D_{11}^{*}D_{22}^{*}-9D_{12}^{*2}\right)\\+\sqrt{D_{11}^{*3}D_{22}^{*}\left(4D_{11}^{*}D_{22}^{*}-3D_{12}^{*2}\right)^3}\end{matrix}\right)^{\frac{1}{2}}.\end{aligned}\tag{39}$$

For the data given in Eqs. (23), (24) this function becomes $R_{\min}=27.08\alpha^{-2}$, where the angle is given in radians and the radius in millimeters. This function perfectly matches the numerical results. The results together with the results of the symmetric layup are shown in Fig. 12. Taking this finding further, if one considers an antisymmetric layup, the various elements of the reduced stiffness matrix would be proportional in some way to the laminate thickness t: $A_{ij}^{*}\sim t$, $B_{ij}^{*}\sim t^2$ and $D_{ij}^{*}\sim t^3$. Making use of this, Eq. (39) can be reordered:

$$R_{\min}\alpha^2/t=const.,\tag{40}$$

which shows that the thickness can also be used to trigger bistable behavior for a given stacking sequence and material properties. If one multiplies Eq. (40) by 1/8, one can see, that for shallow shells the result means, that to achieve bistability with a given material and stacking sequence, the shell height (Z-directional size in Fig. 1) to shell thickness ratio should be greater than a constant value defined by the stacking sequence. This comes from the fact that for small central angles α, the height can be well approximated by its series: $R(1-\cos\alpha/2)\approx R\,\alpha^2/8$.

To examine the result regarding the limiting condition for the bistable behavior given by Eqs. (39), (40), FE simulations were conducted on the [45°, −45°, 0°, 45°, −45°] stacking sequence and the material properties of Material 1, given in Table 1. The minimal radius of the cross-section was found with bisection method for several (α, t) combinations. The results are shown in Fig. 13, on a logarithmic scale. A plane fitting in the logarithmic space with an R^2 value of 0.99958 confirmed that Eq. (40) holds for the FE simulations too. However, the limiting, dimensionless $R_{\min}\,\alpha^2/t$ constant is predicted by Eq. (39) is highly

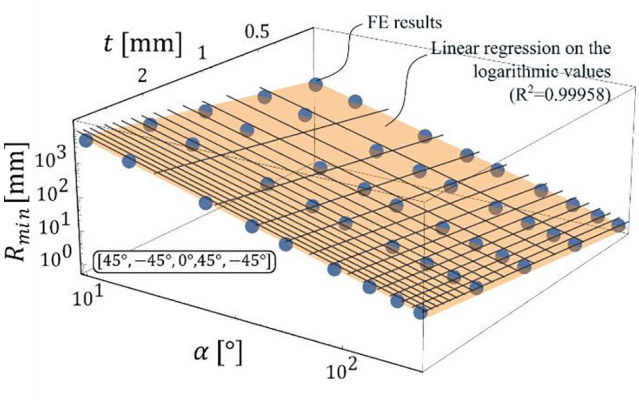

Fig. 13 The FE results for the minimal cross-section radius as a function of cross-section angle and laminate thickness

inaccurate. The analytical, simplified model would yield 25.791, while the fit to the FE results gives 32.8255 (this means a −21.4% relative error for the minimal necessary radius prediction). Although the prediction of Eq. (39) is inaccurate, it showed that to achieve two stable configurations for a cylindrical composite shell with antisymmetric layup, the $R\,\alpha^2/t$ dimensionless parameter should be greater than a certain value, which depends on the layup and material parameters. This means, that this constant is enough to be found accurately for a single parameter combination (i.e. one finds $R_{\min}$ for a given (α; t) point with FE simulations), and then the limiting surface between the mono- and bistable configurations can be determined accurately.

To see how the bistability limit changes with the orientation angle for the antisymmetric layup, it was calculated and plotted for the [0, 90]° interval. The layup in this case is defined as [$-\theta$, θ, 0°, $-\theta$, θ]. The results can be seen in Fig. 13. It can be found that the lowest $R_{\min}$ value will be found at θ = 48.5° for the given layup. As shown above, changing the thickness of the shell does not change the shape of the $R_{\min}\,\alpha^2/t$ curve on a logarithmic scale, only translates it along the vertical axis. The minimum location of the curve will not change to the shell thickness. However, removing the middle layer with the 0° orientation angle makes the shape *almost* symmetrical to θ = 45°. It is important to note, that the laminate thickness was the same (1.05 mm) for both layups investigated in Fig. 14, so that the results can be compared. It is found that that a middle layer with a 0° orientation angle may significantly lower the geometric constant The effect of the layup angle is confirmed by FE simulations (dashed curves in Fig. 14), although if the orientation angle is below 30° and above 60° the shape obtained from FE simulations starts to deviate significantly from the analytical solution. The $R_{\min}\,\alpha^2/t$ constant was found with bisection method for $\theta\in[15°, 70°]$ in 2.5°

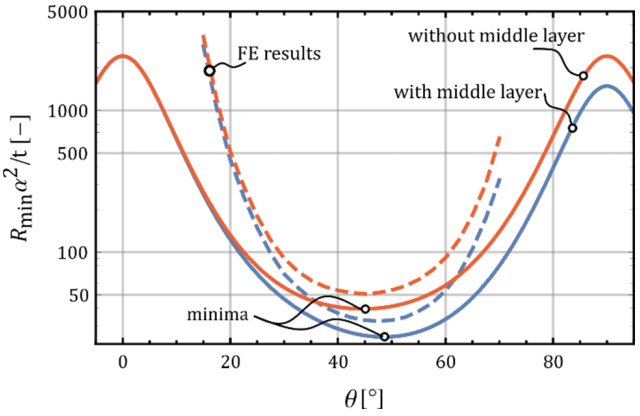

Fig. 14 The layup dependent coefficient in Eq. (37) as a function of the orientation angle for two different layups

steps. The calculations were carried out for $t = 1.05$ mm and $\alpha = \pi/2$, while the radius was varied to find the limit where the minimum of the bending moment function reaches zero in the case of a same sense bending.

Below 15° and above 70° the nonlinearity grows stronger, and no solutions were found due to convergence issues. However, the functions suggest, that these would lie outside the practical region of interest due to the huge dimensions required achieve the minimum constant value.

4.2 Bistability limit of the symmetric layup

For the symmetric layup, the algorithm is the same in general, although one cannot assume that there is no twist in the system. So, one must solve the $T = 0$ equation as in Eq. (33). Now all $k_l^{(i)}$ expressions contain φ. Unfortunately, so far, no closed-form analytical solution was found; thus, the system of equations given by Eqs. (30)–(33) with zero moments was solved numerically for several (R; α) combinations, and the minimal radius was found with bisection method. In the bistable region, the model yields more than two stable configurations; the extra ones can be filtered out by restricting the value of the transverse curvature: $k_t \in (-1,1)$. The results of these calculations are presented in Fig. 12.

In contradiction to the results of Galletly and Guest [1], stable configurations were found for the 45° symmetric stacking sequence, too. It is of importance, that these were found with the $\boldsymbol{K}_s^*$ matrix given in Eq. (24). Interestingly, with the material data used for the FE solution, no bistable domain exists in the $\alpha - R$ plane, although the difference between the two reduced stiffness matrices stems only from rounding errors and could be considered negligible. Unfortunately, since, for the antisymmetric layup no closed form condition of bistability exists, further investigation on this matter cannot be conducted analytically.

5 Conclusion

In this article an investigation was carried out on the effect of the layup on the stability of the composite cylindrical shells. For the investigation, a simple, uniform curvature, flexible cross-section beam model [1] was used, and methods were presented for the analysis of the tape-spring's behavior. Through numerical calculations it was shown, how the snap-through of the shell may disappear for some shell geometries and orientation angles. It is also shown that for certain geometries, the snap-through moment remains practically unchanged for any layup orientation angle. These were also confirmed by the finite element calculations. It is shown, that while the simple, uniform curvature model is inaccurate, it represents well the qualitative behavior of the tape springs. We found that the antisymmetric layup depending on the cross-section geometry may have two separate (one open and one closed) trajectories simultaneously for uniform longitudinal bending. Using this model, it is proven that the flattening of the cross-section is inevitable through layup modification.

Regarding the bistable behavior of the shell, a closed-form analytical solution was derived for the geometrical parameters of the cross-section, which limit the bistable property of the shell. While the analytical solution does not provide an accurate result, the FE calculations confirmed that the on the limiting surface between bistable and monostable behavior the $R\ \alpha^2/t$ remains constant. The effect of the orientation angles on the bistable geometries was also shown. Finite element simulations confirmed that while around 45° layup angles the analytical model yields qualitatively accurate results, below 30° and above 70° the FE simulations start to deviate significantly. These also indicate that while bistability can be achieved theoretically close to 0° and 90° layup angles too, the geometrical parameter combinations lie outside of the region of practical interest.

Acknowledgement

The project presented in this article is supported by the ÚNKP-22-3-II-BME-107 New National Excellence Program of the Ministry for Culture and Innovation and by the National Research, Development and Innovation Office (NRDI) under grant No.134303. The research reported in this paper has been supported by Project no. TKP-6-6/PALY-2021 provided by the Ministry of Culture and Innovation of Hungary from the National Research, Development and Innovation Fund, financed under the TKP2021-NVA funding scheme.

Nomenclature

Roman letters

Notation	Description	Unit
$\boldsymbol{A}$	Laminate extensional stiffness matrix	N/mm
b	Cross-section arc length	mm
$\boldsymbol{B}$	Laminate extensional-bending coupling stiffness matrix	N
$\boldsymbol{C}$	Stiffness matrix of a lamina	MPa
$\boldsymbol{D}$	Laminate bending stiffness matrix	Nmm
E_x	Beam axial strain	–
$\boldsymbol{K}^*$	Reduced stiffness matrix	
$\boldsymbol{K}_0, \boldsymbol{K}_1, \boldsymbol{K}_2$	Submatrices of the laminate stiffness matrix	
K_L	Longitudinal beam curvature	1/mm
K_T	Transverse, cross-section curvature	1/mm
k_l	Dimensionless longitudinal curvature	–
k_t	Dimensionless transverse curvature	–
M_L	Beam longitudinal bending moment	Nm
M_T	Transverse moment on the beam	Nm
M_{st}	Snap-through bending moment	Nmm
M_x, M_y, M_{xy}	Moment resultants of the shell	N
N_x, N_y, N_{xy}	Force resultants of the shell	N/mm
N	Beam normal stress resultant force	N
R	Initial radius of the cross-section	mm
s	Arc-length coordinate of the cross-section	mm
t	Shell, or laminate thickness	mm
T	Beam torsional moment	Nm

Greek letters

Notation	Description	Unit
α	Central angle of the cross-section	rad
δ	Relative error	%
$\varepsilon_x, \varepsilon_y, \varepsilon_{xy}$	Membrane strains	–
θ	Fiber orientation angle	rad or °
$\kappa_x, \kappa_y, \kappa_{xy}$	Bending strains	1/mm
φ	Dimensionless twist	–
ϕ	Beam twist	rad/mm

References

[1] Galletly, D. A., Guest, S. D. "Bistable composite slit tubes. I. A beam model", International Journal of Solids and Structures, 41(16–17) pp. 4517–4533, 2004. https://doi.org/10.1016/j.ijsolstr.2004.02.036

[2] Galletly, D. A., Guest, S. D. "Bistable composite slit tubes. II. A shell model", International Journal of Solids and Structures, 41(16–17) pp. 4503–4516, 2004. https://doi.org/10.1016/j.ijsolstr.2004.02.037

[3] Rimrott, F. P. J. "Storable tubular extendible members", Machine Design, 37, pp. 156–165, 1965.

[4] Wuest, W. "Einige Anwendungen der Theorie der Zylinderschale" (Some applications of the theory of the cylindrical shells), ZAMM - Journal of Applied Mathematics and Mechanics / Zeitschrift für Angewandte Mathematik und Mechanik, 34(12), pp. 444–454, 1954. (in German)

[5] Martin, M., Bourgeois, S., Cochelin, B., Guinot, F. "Planar folding of shallow tape springs: The rod model with flexible cross-section revisited as a regularized Ericksen bar model", International Journal of Solids and Structures, 188–189, pp. 189–209, 2020. https://doi.org/10.1016/j.ijsolstr.2019.10.009

[6] Ericksen, J. L. "Equilibrium of bars", Journal of Elasticity, 5(3–4), pp. 191–201, 1975. https://doi.org/10.1007/bf00126984

[7] Kebadze, E., Guest, S. D., Pellegrino, S. "Bistable prestressed shell structures", International Journal of Solids and Structures, 41(11–12), pp. 2801–2820, 2004. https://doi.org/10.1016/j.ijsolstr.2004.01.028

[8] Iqbal, K., Pellegrino, S., Daton-Lovett, A. "Bistable composite slit tubes", In: IUTAM-IASS Symposium on Deployable Structures: Theory and Applications, Cambridge, UK, 2000, pp. 153–162. ISBN 978-90-481-5539-2 https://doi.org/10.1007/978-94-015-9514-8_17

[9] Iqbal, K., Pellegrino, S. "Bi-stable composite shells", In: 41st Structures, Structural Dynamics, and Materials Conference and Exhibit, Atlanta, GA, USA, 2000, AIAA 2000-1385. https://doi.org/10.2514/6.2000-1385

[10] Wang, B., Seffen, K., Guest, S. "Folding of a bistable tape-spring structure based on plain-woven composite", Apollo – University of Cambridge Repository, 2019. https://doi.org/10.17863/CAM.36526

[11] Lee, H., Lee, J.-G., Ryu, J., Cho, M. "Twisted shape bi-stable structure of asymmetrically laminated CFRP composites", Composites Part B: Engineering, 108, pp. 345–353, 2017. https://doi.org/10.1016/j.compositesb.2016.09.079

[12] Yang, C., Wang, B., Zhong, S., Zhao, C., Liang, W. "On tailoring deployable mechanism of a bistable composite tape-spring structure", Composites Communications, 32, 101171, 2022. https://doi.org/10.1016/j.coco.2022.101171

[13] Seriani, S., Gallina, P. "A Storable Tubular Extendible Member (STEM) parallel robot: Modelization and evaluation", Mechanism and Machine Theory, 90, pp. 95–107, 2015. https://doi.org/10.1016/j.mechmachtheory.2015.03.010

[14] Vidoli, S. "Discrete approximations of the Föppl–Von Kármán shell model: From coarse to more refined models", International Journal of Solids and Structures, 50(9), pp. 1241–1252, 2013. https://doi.org/10.1016/j.ijsolstr.2012.12.017

[15] Brunetti, M., Vincenti, A., Vidoli, S. "A class of morphing shell structures satisfying clamped boundary conditions", International Journal of Solids and Structures, 82, pp. 47–55, 2016. https://doi.org/10.1016/j.ijsolstr.2015.12.017

[16] Brunetti, M., Kloda, L., Romeo, F., Warminsky, J. "Multistable cantilever shells: Analytical prediction, numerical simulation and experimental validation", Composites Science and Technology, 165, pp. 397–410, 2018. https://doi.org/10.1016/j.compscitech.2018.06.021

[17] Brunetti, M., Mitura, A., Romeo, F., Warminski, J. "Nonlinear dynamics of bistable composite cantilever shells: An experimental and modelling study", Journal of Sound and Vibration, 526, 116779, 2022.
https://doi.org/10.1016/j.jsv.2022.116779

[18] Mitura, A., Brunetti, M., Kloda, L., Romeo, F., Warminski, J. "Experimental nonlinear dynamic regimes for energy harvesting from cantilever bistable shells", Mechanical Systems and Signal Processing, 206, 110890, 2024.
https://doi.org/10.1016/j.ymssp.2023.110890

[19] Guinot, F., Bourgeois, S., Cochelin, B., Blanchard, L. "A planar rod model with flexible thin-walled cross-sections. Application to the folding of tape springs", International Journal of Solids and Structures, 49(1), pp. 73–86, 2012.
https://doi.org/10.1016/j.ijsolstr.2011.09.011

[20] Picault, E., Marone-Hitz, P., Bourgeois, S., Cochelin, B., Guinot, F. "A planar rod model with flexible cross-section for the folding and the dynamic deployment of tape springs: Improvements and comparisons with experiments", International Journal of Solids and Structures, 51(18), pp. 3226–3238, 2014.
https://doi.org/10.1016/j.ijsolstr.2014.05.020

[21] Reddy, J. N. "Mechanics of laminated composite plates and shells: Theory and analysis", CRC Press, 2004. ISBN 9780849315923

[22] Máté, P., Szekrényes, A. "Stability analysis of thin cylindrical shells under pure and three-point bending", Mathematics and Mechanics of Solids, 2024.
https://doi.org/10.1177/10812865241259134